

# Synthesis, characterization, material properties and sensor application study of polyaniline/niobium doped titanium dioxide nanocomposites

M. T. Ramesan<sup>1</sup>  · T. Sampreeth<sup>1</sup>

Received: 20 May 2017 / Accepted: 11 July 2017 / Published online: 17 July 2017  
© Springer Science+Business Media, LLC 2017

**Abstract** Conducting polyaniline (PANI)/niobium doped titanium dioxide (Nb–TiO<sub>2</sub>) nanocomposites with different weight percentages of Nb–TiO<sub>2</sub> nanoparticles were synthesized by an in situ polymerization method. The synthesized materials were characterized by FT-IR, UV, XRD, SEM, HRTEM, TGA, DSC and electrical conductivity measurements. Also, the ammonia gas sensing properties of PANI and its nanocomposites have been explored thoroughly. The FT-IR and UV spectra showed the clear evidences for the presence of nanoparticles by shifting to a broad peak, which indicates the interaction of nanoparticles with PANI. The XRD study reveals the crystalline nature of the fabricated nanocomposite. SEM and TEM analysis indicates the uniform dispersion of nanoparticles in the polymer matrix with spherically shaped particles having the nano-size region. TGA analysis showed the increased thermal stability of nanocomposites with an increase in concentration of nanoparticles. The increase in glass transition and melting temperature with the increase in content of nanoparticles were obtained from DSC. Both AC and DC conductivity and dielectric properties of the nanocomposites were increased with the increase in content of nanoparticles and the maximum electrical properties were obtained for 10 wt% of composite. The fabricated composites showed excellent sensitivity and fast response to ammonia gas at room temperature. The effect of nanoparticles in the polymer chain increases the potential application of the conducting polyaniline, can act as multifunctional promising new material such as nanoelectronic devices and sensors.

## 1 Introduction

During the last few decades, conducting polymers have opened up a promising field in material science and engineering because of conducting polymer nanocomposites with metal oxide nanoparticles have enormous potential applications in sensors, energy storage devices, electrochromic devices, membrane gas separation and so on [1–4]. Recently several studies have been carried out in progress with the fabrication and characterization of hybrid conducting polymeric material with inorganic nanoparticles as filler to enhance the mechanical behavior of conducting polymers. Among the conducting polymers, polyaniline (PANI) has been received a great attention due to its ease of synthesis, electrical and optical properties, low cost, unique doping/de-doping behavior and good stability [5–7]. It has been studied for a wide range of active materials like novel biosensors, energy storage devices and electrical devices [8–11]. The oxidation and protonation determines PANI'S electrical conductivity. However the only conducting form of PANI is its emeraldine base (EB) and it can be highly conductive when protonated. The conductivity of PANI is high as 10<sup>2</sup> S/cm [12].

Recently PANI with various inorganic nanomaterials has been investigated extensively because their properties are quite different from the isolated polymer chain [13]. However the applicability of conducting polymer remains limited because of its lack of processability and poor mechanical strength. The irregular structure of conducting polymers makes quite difficult in the investigation of conducting polymer. Nevertheless, to improve the structure and property the only possible way is to prepare polymer blend or composite materials with amazing properties [14–18]. Also the conducting polymer nanocomposites having metal oxide nanoparticles with organized structures has received

✉ M. T. Ramesan  
mtramesan@uoc.ac.in

<sup>1</sup> Department of Chemistry, University of Calicut, Calicut, Kerala 673 635, India

much attention due to their unique electrical properties and potential applications in several areas such as non-linear optics and electrochromic devices [19, 20]. Hence the combination of polymer matrix with nanoparticles allows the formation of new material with specific electrical properties.

Titanium dioxide is a non-stoichiometric compound that exhibits interesting photochemical properties. The band gap of  $\text{TiO}_2$  is 3.2 eV and it is an amphoteric semiconductor. It can act as p-type or n-type properties at low and high oxygen activities. The electrical conductivity of materials are improved by doping of  $\text{TiO}_2$  with Nb and this is attributed to the vacancy available in Ti atoms [21, 22]. Several methods are used for the fabrication of conducting polymer blends or composites such as solution mixing, melt mixing, and chemical synthesis. The negative aspect of all these methods are the nanoparticles undergoes agglomeration inside the polymer matrix. The agglomeration or the poor dispersion of nanoparticles within the polymer can be much reduced by the in situ polymerization of monomer with metal oxide nanoparticles [23]. Here we report the synthesis of PANI/Nb– $\text{TiO}_2$  nanocomposite with respect to different contents of nanoparticles and the prepared materials were characterized by FT-IR, UV–Vis, SEM, HRTEM, TGA, DSC and AC and DC conductivity studies. The sensitivity of the metal oxide nanoparticles reinforced with PANI matrix for detecting gaseous ammonia was also evaluated.

## 2 Experimental

### 2.1 Materials and methods

Aniline (Merck) was purified by double distillation under reduced pressure. The oxidant, ammonium persulfate (APS) (Merck), HCl, titanium isopropoxide  $\text{Ti}(\text{OPr})_4$  (Aldrich), niobium pentoxide ( $\text{Nb}_2\text{O}_5$ ) (Aldrich), glacial acetic acid (Aldrich), cetyl trimethyl ammonium bromide (CTAB) (Merck), were used to synthesize the material without further purification. De-ionized water is used for all synthesis.

### 2.2 Synthesis of polyaniline

Polyaniline (PANI) was synthesized by using chemical oxidation method. An appropriate amount of aniline and 1 M HCl were mixed together and stirred for 5 min. Required amount of ammonium persulfate (APS) as an oxidizing agent was added drop by drop to this solution till polymerization took place and the reaction mixture was stirred for 10 h. with constant magnetic stirring at low temperature (0–5 °C). The polymer obtained was filtered, washed

several times with de-ionized water, ethanol, finally by dilute HCl. The precipitate was dried at 60 °C for 6 h. to obtain green powder of PANI.

### 2.3 Preparation of Nb doped $\text{TiO}_2$ nanoparticles

Niobium doped  $\text{TiO}_2$  nano-powder was synthesized via sol–gel method [22]. The  $\text{Ti}(\text{OPr})_4$  was treated with glacial acetic acid followed by the addition of deionized water in small quantity with constant stirring. To this 2 wt% of niobium pentoxide ( $\text{Nb}_2\text{O}_5$ ) was added. The  $\text{Ti}(\text{OPr})_4$ : acetic acid: water ratio was kept as 1:10:100. The homogeneous solution was stirred for 3 h. It was dried at 100 °C on water bath for 12 h. The dried powder was calcined at 500 °C at a heating rate of 5 °C per minute and held at this temperature for 2 h and immediately stored in a desiccator.

### 2.4 Synthesis of PANI/Nb doped $\text{TiO}_2$ nanocomposites

The PANI/Nb– $\text{TiO}_2$  nanocomposites were synthesized by in situ polymerization technique. Nanoparticles with various concentrations (0, 3, 5, 7, 10 and 15 wt%) was added to the aqueous solution of aniline monomer in 1 M HCl and CTAB with continuous stirring and the reaction mixture was ultrasonicated over a period of 20 min. After sonication, required quantity of ammonium persulfate [ $(\text{NH}_4)_2\text{S}_2\text{O}_8$ ] was added to the mixture by drop wise at a reaction temperature of 0–5 °C and carried out the polymerization for 10 h with constant stirring. The precipitate formed was filtered and washed with water, ethanol, finally with dil. HCl and dried under vacuum at a temperature of 60 °C for 24 h.

### 2.5 Characterization

The Fourier Transform Infrared (FT-IR) spectra of the samples were recorded by using a JASCO (Model 4100) Fourier Transform Infrared spectrophotometer in the region of 4000–400  $\text{cm}^{-1}$ . The UV–Vis absorption spectra of the synthesized PANI and PANI nanocomposites with different contents of Nb doped  $\text{TiO}_2$  nanoparticles in dimethyl sulfoxide were recorded by using Perkin Elmer Lambda 650 spectrophotometer in the wavelength of 200–800 nm. The X-ray diffraction studies of the synthesized material were recorded on Bruker AXS D X-ray diffractometer using  $\text{CuK}\alpha$  radiation ( $k=1.5406 \text{ \AA}$ ) with an accelerating voltage of 30 KV. The diffractograms were recorded in the range of  $2\theta=10^\circ\text{--}80^\circ$  at a speed rate of  $2^\circ/\text{min}$ . The scanning electron micrographs (SEM) images of the fabricated polymer nanocomposites were investigated by Hitachi S-3000H scanning electron microscope. The structure of composite was analyzed by high resolution transmission electron microscopy (HRTEM-JEOL/JEM 2100).

The specimen for HRTEM analysis was obtained using the droplet of PANI/Nb–TiO<sub>2</sub> nanocomposites in solution on the surface of carbon coated copper grid and then air dried for 2 h. Thermal analysis of the material was studied by Hitachi STA7200 thermogravimetric analyzer with pure nitrogen gas at a heating rate of 10 °C min<sup>-1</sup>. DSC studies of the PANI and PANI/Nb–TiO<sub>2</sub> were carried out on TA instrument DSC-Q 20. The samples were heated at a rate of 10 °C min<sup>-1</sup> (atmosphere N<sub>2</sub>; flow 40 mL/min). The electrical conductivity and dielectric properties of the samples were studied by using a Hewlett Packard LCR meter (HP 4284A), fully automatic system in frequency range of 10<sup>2</sup>–10<sup>6</sup> Hz at room temperature. DC conductivity of the material was carried out on Keithly 2400, full automatic system. The gas sensing characteristics of the PANI/Nb–TiO<sub>2</sub> nanocomposites were measured as a function of exposing time of ammonia gas. The composite in the form of pellet was placed on silver plate inside the glass test chamber (500 ml) with an inlet and an outlet for the gas. Ammonia gas (100 ppm) was passed into the chamber and the gas sensitive characteristics were recorded by measuring the resistance when pellet was exposed to ammonia at room temperature using a multi-function digital multimeter (MECO Meters Pvt. Ltd., Mumbai, India). After each sensing cycle, the test gas was evacuated from the outlet and the sensor was placed in atmospheric air for recovery. The sensitivity or response of the sensor is defined as  $(R_i - R_0)/R_0$ , where  $R_i$  and  $R_0$  are the resistance of sensors in ammonia and in air, respectively. Each data of the gas sensitivity were collected by three time measurement and average values were calculated. All experiments were carried out at room temperature.

### 3 Results and discussion

#### 3.1 FT-IR spectroscopy

Figure 1 shows the FT-IR spectra of PANI/Nb doped TiO<sub>2</sub> and the composite with 5 and 10 wt% nanoparticles incorporated PANI. The major peak of PANI at 3426 cm<sup>-1</sup> corresponds to the NH stretching vibration. The C=C bond stretching of quinoid and benzenoid ring of PANI are located at 1563 and 1473 cm<sup>-1</sup> respectively. The peak obtained at 1297 is attributed to the C–N stretching and the in plane bending of C–H bond appears at 1332 cm<sup>-1</sup>. The absorption band at 798 cm<sup>-1</sup> is the out-of-plane bending vibration of C–H which confirms the formation of PANI [24]. The FT-IR spectra of Nb–TiO<sub>2</sub> showed the strong absorption band at 665 cm<sup>-1</sup> and another at 1033 cm<sup>-1</sup>, are corresponding to the Ti–O–Ti and Ti–O bands respectively. The curve also exhibited the peaks around 3431 and 1627 cm<sup>-1</sup> are related to the stretching and bending

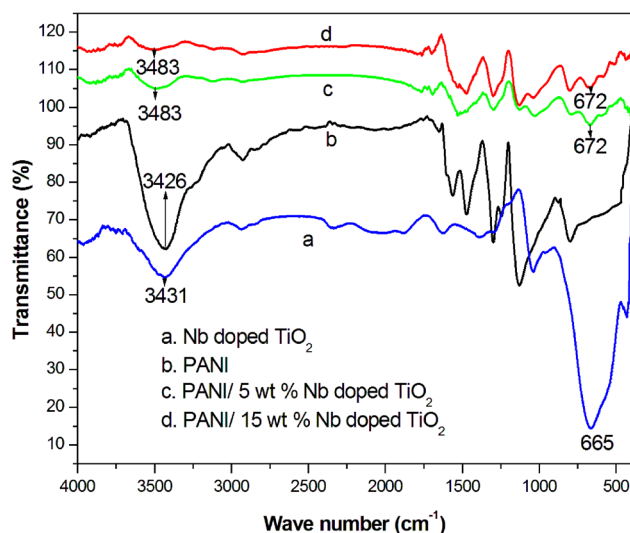


**Fig. 1** FTIR spectra of Nb–TiO<sub>2</sub>, PANI and PANI with different contents of Nb doped TiO<sub>2</sub> nanoparticles

vibration of hydroxyl group present in the surface of metal oxide particles. However, the spectrum of PANI/Nb–TiO<sub>2</sub> showed the characteristic absorption bands of PANI with the formation of new peak at 672 cm<sup>-1</sup>, which is the characteristic Ti–O bond stretching [25] indicating the presence of Nb–TiO<sub>2</sub> in PANI. It can be seen from the figure that the NH band of PANI at 3426 cm<sup>-1</sup> is found to be shifting to a higher wavenumber at 3483 cm<sup>-1</sup> by the insertion of nanoparticles. Interestingly the C=C bond stretching of PANI at 1563 and 1473 cm<sup>-1</sup> are overlapped and merge to a absorption band at 1524 cm<sup>-1</sup>. These shifts in absorption frequencies of composite as compared to pure PANI is due to the strong interfacial interactions between the nanoparticles and the polar segment of PANI. Hence it can be concluded that the aniline monomers are successfully polymerized on the surface of Nb–TiO<sub>2</sub>.

#### 3.2 UV–Vis spectra

The UV–Vis spectra of PANI and different concentrations of Nb doped TiO<sub>2</sub> /PANI nanocomposites are shown in Fig. 2. In the UV spectra of PANI, three absorption peaks are observed at 260, 287 and 344 nm. The major peak at 260 nm is the n–π\* transition of PANI and the second peak at 287 nm is related to the π–π\* transition of benzenoid ring. The third UV absorption peak at 344 nm is the excited absorption of quinoid ring. These UV absorption peaks indicates the polymerization of aniline, which was similar to that of the earlier study [26]. In the case of nanocomposite, the UV absorption peak of PANI is shifting to a higher wavelength region. The interfacial interaction between the nanoparticles and the polymer chain is responsible for the shift in the absorption peak of PANI/Nb–TiO<sub>2</sub> composite.

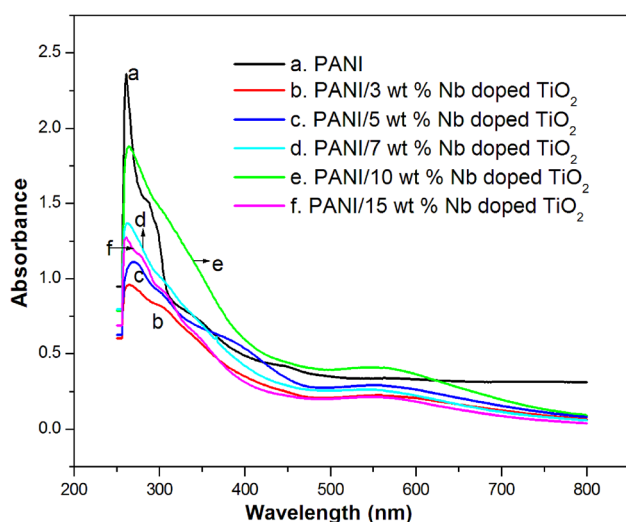


**Fig. 2** UV–Visible spectra of PANI and its composites with different contents of Nb doped TiO<sub>2</sub> nanoparticles

Among the nanocomposites, the sample with 10 wt% of Nb–TiO<sub>2</sub> shows the maximum intensity with an increase in broadness of peak from the entire range from 200 to 600 nm. The higher broadness and intensity of the composite is due to the uniform dispersion of nanoparticles within the macromolecular chain of PANI. However, the intensity and broadness of UV peak decreases beyond 10 wt% loading. This is due to the aggregation or formation of clusters in the PANI matrix, which suppress the light energy to pass through the materials.

### 3.3 X-ray diffraction analysis (XRD)

The structure and interactions of PANI with different contents of Nb doped TiO<sub>2</sub> nanoparticles are monitored by X-ray diffraction studies. The XRD curve of Nb doped TiO<sub>2</sub>, PANI and its composite with different contents of Nb–TiO<sub>2</sub> nanoparticles are given in Fig. 3. The synthesized nanoparticles shows the crystalline diffraction peaks at  $2\theta = 27.05^\circ$ ,  $35.54^\circ$ ,  $41.25^\circ$ ,  $54.33^\circ$ ,  $56.61^\circ$  and  $69.02^\circ$  are the scattering from (101), (103), (112), (105), (211) and (214) planes of the crystal lattice of Nb doped TiO<sub>2</sub> respectively [27]. XRD pattern of PANI shows a broad amorphous peak at  $2\theta = 25.22^\circ$  along with a weak peak at  $2\theta = 20.75^\circ$  riding over the broad hump, representing the scattering from (100), (110) planes of PANI respectively [28]. Comparing the XRD pattern of PANI/Nb–TiO<sub>2</sub> nanocomposites with pure PANI, it can be observed that the broadness and intensity of the amorphous peak of PANI is reduced with an increase in concentration of Nb–TiO<sub>2</sub> nanoparticles. The decrease in amorphous nature of PANI with the addition of metal oxide nanoparticles reveals that the structure of PANI is strongly affected by the encapsulation

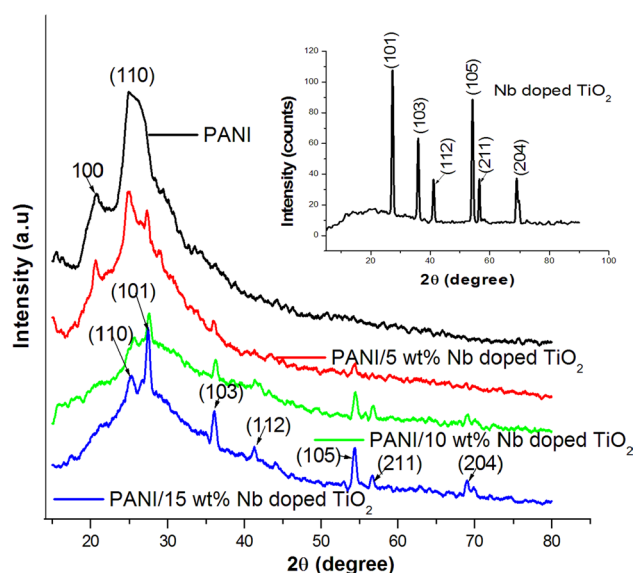


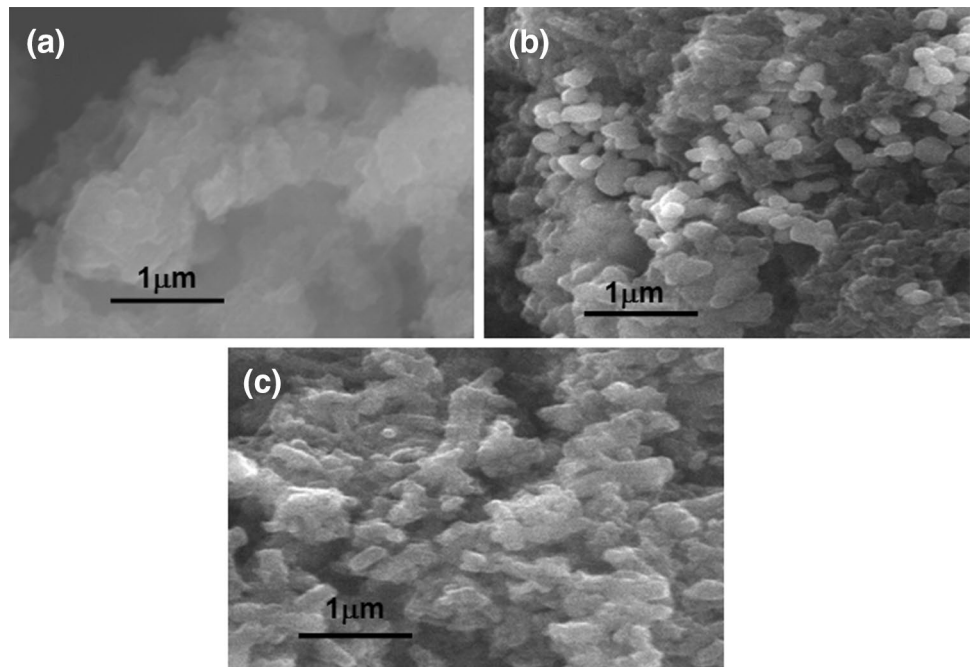
**Fig. 3** XRD patterns of Nb–TiO<sub>2</sub>, PANI and PANI with different contents of Nb–TiO<sub>2</sub> nanoparticles

of nanoparticles. It can also be observed from the figure that the major amorphous peak of PANI ( $2\theta = 25.16^\circ$ ) is slightly shifted to a lower diffraction angle at  $2\theta = 24.89^\circ$ . This shift in diffraction peak increases the interlayer volume of the nanocomposite. PANI/Nb–TiO<sub>2</sub> composite exhibits most of the diffraction peak of nanoparticles and the intensity of the XRD peak increases with the increase in content of Nb–TiO<sub>2</sub>. The ordered arrangement of nanoparticles within the PANI matrix is due to the strong intermolecular interactions between the titanium atom and nitrogen of PANI.

### 3.4 Scanning electron microscopy (SEM)

The surface morphology of pure PANI and PANI with different contents of Nb doped TiO<sub>2</sub> nanocomposites were characterized by SEM and the SEM images are given in Fig. 4. The surface morphology of pure PANI is relatively porous structure with irregular shape. However, the surface morphology of composite with 7 wt% sample shows the uniform dispersion of nanoparticles with good uniformity and adhesiveness and that leads to spherically shaped nanoparticles. The uniform morphology of the nanocomposite is due to the overlapping of empty 3d orbital of titanium with the nitrogen atoms of PANI. Additionally, the polar nanoparticles have large surface area, which can effectively interact with the polar segments of PANI. When the loading of nanoparticles became 15 wt%, the surface morphology of the composite is significantly changed due to the agglomeration of nanoparticles and also the stress developed in the composites leads to the poor dispersion of filler particles inside the PANI matrix. Hence it can be

**Fig. 4** SEM images of **a** PANI, **b** PANI/7 wt% Nb–TiO<sub>2</sub> and **c** PANI/15 wt% Nb–TiO<sub>2</sub>



concluded that lower concentration of nanoparticles can effectively form core–shell architecture.

### 3.5 High resolution transmission electron microscopy (HRTEM)

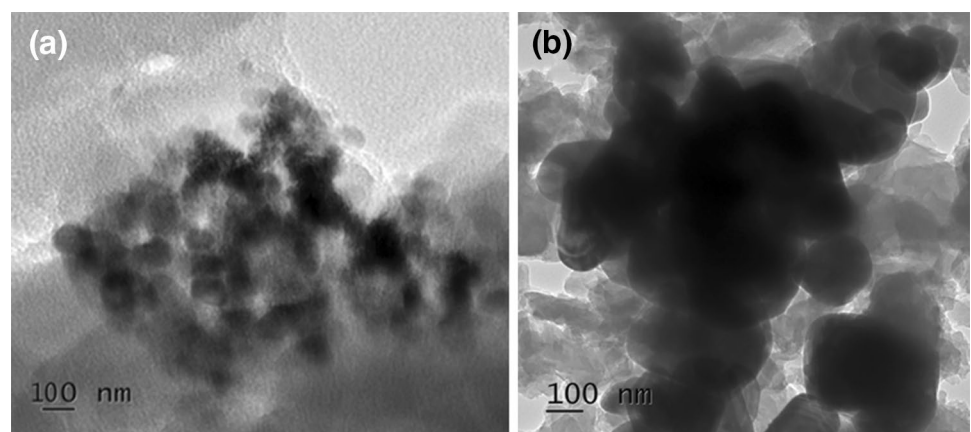
The HRTEM images of polyaniline nanocomposite with different concentrations (7 and 15 wt%) of Nb doped TiO<sub>2</sub> nanoparticles are given in Fig. 5. TEM images of 7 wt% sample reveals that PANI chain are adsorbed on the surface of Nb doped TiO<sub>2</sub> nanoparticles having spherically shaped particles with average particle diameter below 100 nm. The uniform dispersion of nanoparticles in the polymer is due to the strong intermolecular interactions between the nanoparticles and the polymer chain. Additionally the monomer molecules are uniformly polymerized on the surface of Nb

doped TiO<sub>2</sub> particles and that leads to a regular polymeric nanostructures. However, when the concentration of nanoparticles reached to 15 wt%, the uniform structure of nanocomposite is totally changed into an irregular morphology with few elongated structure. The change in morphology is due to the formation of cluster or aggregates which arises from the poor interfacial interactions between the nanoparticles and the PANI matrix.

### 3.6 Differential scanning calorimetry (DSC)

The glass transition temperature ( $T_g$ ) of PANI and its nanocomposites with respect to different concentration of Nb doped TiO<sub>2</sub> nanoparticles is shown in Fig. 6. It is well known that the glass transition temperature is appears as a sudden change in slope in the DSC curve or with an

**Fig. 5** HRTEM photographs of **a** PANI/7 wt% Nb–TiO<sub>2</sub> and **b** PANI/15wt% Nb–TiO<sub>2</sub>



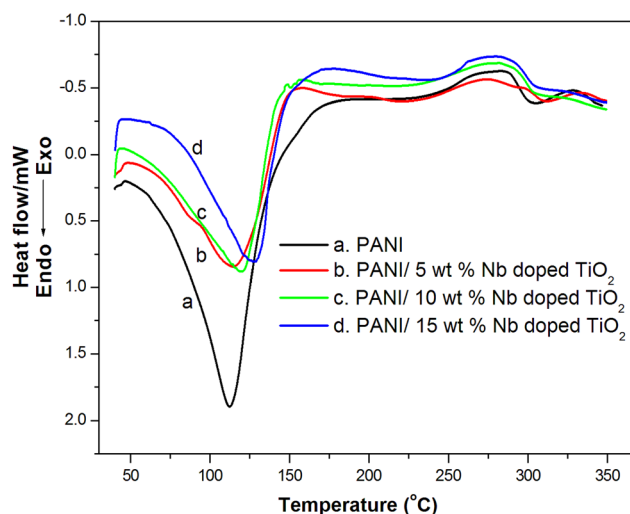


**Fig. 6** DSC profile of PANI and its composite with different loading of Nb–TiO<sub>2</sub> nanoparticles

endothermic dip at lower temperature. It can be observed from the figure that the PANI (Fig. 5.6 a) shows a broad endothermic dip at 111 °C, is the glass transition temperature of virgin polymer and a weak deflection at 222 °C is the melting temperature of PANI. The  $T_g$  value of PANI/Nb–TiO<sub>2</sub> nanocomposites with 5, 10 and 15 wt% Nb–TiO<sub>2</sub> nanoparticles are appears at 114, 120 and 128 °C respectively. Similarly the melting temperature ( $T_m$ ) of 5, 10 and 15 wt% composites are appears at 228, 236 and 242 °C respectively. The increase in  $T_g$  and  $T_m$  of nanocomposites are due to the restriction of polymer chain mobility.  $T_g$  of a polymer composite depends on the free volume movement of polymer chain, and the interaction between the polymer and filler particles. Here the increase in  $T_g$  and  $T_m$  of nanocomposites are mainly due to the strong interaction between Nb doped TiO<sub>2</sub> and the polymer chain. The higher affinity of polymer to nanoparticles leads to the ordered arrangement of nanoparticles within the polymer matrix, which is already confirmed from the XRD studies. Therefore the uniform structure of polymer composite gives a regular packing of polymer chain and thereby result in higher  $T_g$  and  $T_m$  of the composites [29]. Therefore it can be inferred that the thermal properties such as  $T_g$  and  $T_m$  depend on the concentration of doped metal oxides in PANI.

### 3.7 Thermogravimetric analysis (TGA)

The thermal degradation behavior of PANI and its nanocomposites with varying concentration of Nb doped TiO<sub>2</sub> nanoparticles have been analyzed by TGA and is given in Fig. 7. There are three steps for the thermal degradation of PANI and its composite with 5, 10 and 15 wt% of Nb–TiO<sub>2</sub>. The first weight loss located between ambient temperature

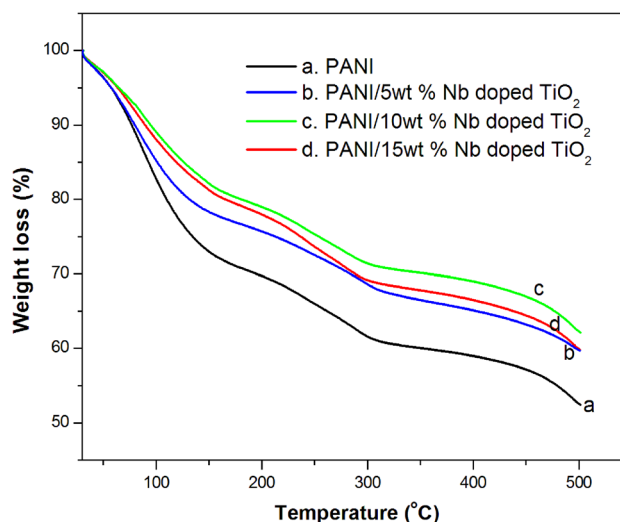
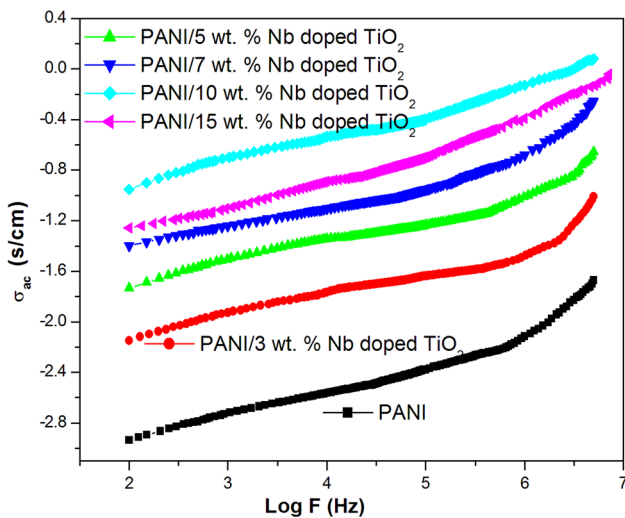


**Fig. 7** TGA patterns of PANI and PANI with different contents of Nb doped TiO<sub>2</sub> nanoparticles

and 180 °C, is due to the loss of free adsorbed and inter-layer water molecules. The second weight loss in the range of 200–320 °C is possibly due to the removal of oligomer and unreacted monomer. The third weight loss starting from 430 °C is attributed to the degradation of organic species constraint within the crystalline region of nanoparticles. It can be seen from the figure that PANI degrades freely at a temperature ranging from 400 to 500 °C. However the decomposition rate of composite is slow as compared to pure PANI and the decomposition temperature of PANI/Nb–TiO<sub>2</sub> nanocomposites are much higher than the pure polymer. The increase in thermal stability of the composite with increase in concentration of nanoparticle is due to the strong interfacial interactions between the nanoparticles and the polymer chain [30]. The magnitude of interaction in 15 wt% composite is poor as compared to 10 wt% Nb–TiO<sub>2</sub> and therefore difference in degradation is almost same. This is due to the agglomeration of nanoparticles and also the poor interaction in the nanocomposite as depicted by the SEM images discussed earlier in this paper. PANI showed 52.04% weight loss at 500 °C while the char residue remains for 10 wt% composite at 500 °C is 66.38%. The observed increase in char residue after the decomposition of nanocomposite indicates the better thermal resistance of PANI/Nb–TiO<sub>2</sub>.

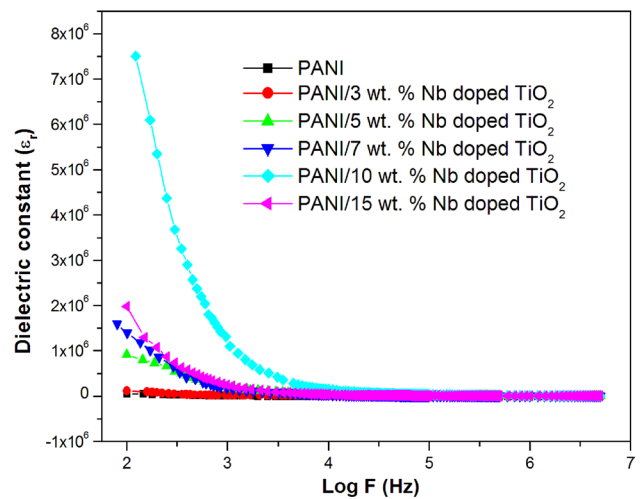
### 3.8 AC conductivity

Figure 8 shows the variation of AC conductivity with frequency at room temperature for different contents of Nb–TiO<sub>2</sub> incorporated PANI. In the present study, the conductivity values of composites have been found to be much greater than pure PANI. It has been reported that the



**Fig. 8** Variation of AC conductivity of PANI with various concentrations of Nb doped TiO<sub>2</sub> nanoparticles

conductivity of conducting polymer composite depends on several factors such as conductivity of filler particles, morphology of the composite, crystallinity and the interfacial adhesion between the nanoparticles and the polymer matrix. Here the higher conductivity of nanocomposite is due to the uniform dispersion of nanoparticles inside the PANI matrix (which is evident from SEM analysis) and the regular arrangement of components leading to higher conductivity. It can be observed from the figure that the conductivity of the composite increases with increase in concentration of nanoparticles up to 10 wt% of Nb–TiO<sub>2</sub> and thereafter the conductivity decreases with further addition of nanoparticles into the polymer matrix [31]. This suggests that the 10 wt% loading brought for the efficient interfacial interaction between the nanoparticles and the polymer chain. These interactions improve the link between the grains and coupling through grain boundaries became the maximum at 10 wt% loading. The decrease in conductivity beyond 10 wt% loading is to the poor dispersion of nanoparticles within the PANI matrix. The presence of various aggregates developed in the PANI, which in turn decreases the particle to particle contact and therefore the available surface area of nanoparticles for the reaction with PANI segments decreases and that leads to poor conductivity. It is also evident from the figure that the conductivity of the sample increases with the frequency indicating the formation of excess charge carriers (polarons and bipolarons) [32]. The frequency dependent conductivity is nearly due to interface charge polarization along with the intrinsic electric dipole polarization. The excellent electrical properties suggest that the in situ polymerized PANI/Nb–TiO<sub>2</sub> has potential application in the field of nanotechnology and multifunctional materials in various electronic devices.



**Fig. 9** Frequency dependence of dielectric constant of PANI with different concentrations of Nb doped TiO<sub>2</sub> nanoparticles

### 3.9 Dielectric constant

The dielectric constant is the measure of the ability of material to store electrical energy. The dielectric constant of PANI and PANI with different contents of Nb doped TiO<sub>2</sub> nanoparticles, are measured at different frequency ranging from 100 to 10<sup>6</sup> Hz and is given in Fig. 9. The dielectric constant of all the samples are steeply decreases with the frequency and reaches a constant value at 10<sup>4</sup> Hz. The dielectric constant of polymeric material depends on the polarization of the dipoles. At lower frequencies, the dipolar units get enough time to arrange themselves in the polymer by the application of electric field and hence the dielectric values are always higher. But at higher frequencies, the orientation of dipoles unit is difficult and therefore the dielectric constant became constant. It is clear from the figure that the dielectric constant of PANI/Nb–TiO<sub>2</sub> composite is much greater than pure PANI. The dielectric value of composite increases with the loading of nanoparticles and the maximum dielectric property is observed for 10 wt% composite. The high dielectric values are mainly due to the efficient intermolecular interaction between the nanoparticles and polymer chain [33]. Moreover, the interfacial polarization leads to an increase in dielectric value and this interfacial polarization increases the movement of virtual charges and these charges get trapped in the interfaces of the components. The interfacial polarization contributed to the increase in dielectric value of the composite. However the dielectric constant is found to be decreases at higher loading of nanoparticles (15 wt%). The large volume fraction of interfaces in the nanocomposite resists the migration of virtual charges. In another aspect the particle to particle distance is reduced

at higher loading which enhances the formation of clusters in the polymer matrix. This in turn reduces the chain mobility, so the effective dielectric property decreases at higher concentration of nanoparticles.

### 3.10 Dielectric loss

The dielectric loss ( $\tan \delta$ ) of composite is commonly associated with the electrical conductivity angle  $\delta$  which is the angle between the vector for the amplitude of charging current and the tangent of this angle is the loss tangent. The  $\tan \delta$  value of PANI with various contents of Nb doped  $\text{TiO}_2$  nanoparticles is presented in Fig. 10. It can be seen that the  $\tan \delta$  values of composites are greater than pure PANI. The variation in  $\tan \delta$  values of all the samples follow the same trend i.e., the dielectric property increases with increase in frequency up to  $10^4$  Hz and thereafter the  $\tan \delta$  value decreases and reaches a constant value at  $10^6$  Hz. Another interesting observation is that the broadness and intensity of the  $\tan \delta$  peaks are much higher than pure PANI, indicating the increased semi crystalline nature of the composite. The composite with 10 wt% sample shows the maximum dielectric loss and beyond 10 wt% loading, the  $\tan \delta$  value decreases (15 wt%). The high value of the  $\tan \delta$  revealed the interaction of polar PANI with the stable and crystalline Nb doped  $\text{TiO}_2$  nanoparticles therefore the synergetic interaction leads to different relaxation phenomena in the polymer composite. However at higher concentration of filler particles (15 wt%), the synergetic interaction decreases due to the presence of small amount of discrete aggregates in the polymer matrix [34].

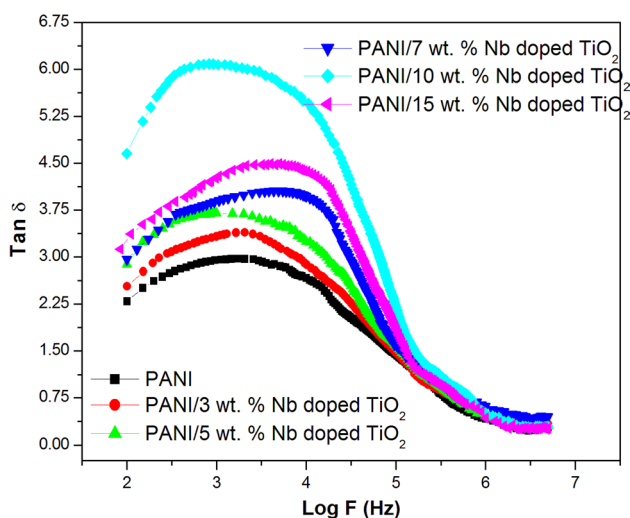


**Fig. 10** Dielectric loss tangent versus frequency plots for PANI with Nb doped  $\text{TiO}_2$  nanoparticles

### 3.11 DC conductivity

Metal oxide nanoparticles have been considered as the best conductive filler particles for converting an insulating polymer to conductive polymeric materials. The plot of DC conductivity of PANI and its nanocomposite with different content of Nb doped  $\text{TiO}_2$  nanoparticles are presented in Fig. 11. All the compounds show a linear variation of electric current with applied voltage. The linear variation is an indication of the semi-crystalline of the matrix. It is evident from the figure that the conductivity of nanocomposites is much greater than that of pure PANI and the magnitude of conductivity increases with the increasing concentration of Nb– $\text{TiO}_2$  nanoparticles. The various factors affecting the conductivity are the polarity and crystallinity of nanoparticles, number of charge carrier or ions, mobility of polymer chain and the quality of electrical network of the system [35]. Here the in situ polymerization of aniline monomer on the surface of Nb doped  $\text{TiO}_2$  nanoparticles leads to a strong interfacial interaction between the crystalline nanoparticles and the polar groups of polyaniline. The interfacial interaction accelerates the charge transport through an electron tunneling process. The high DC conductivity value is noted for 10 wt% composite, which indicates the higher interface contact of metal oxide nanoparticles with the polymer segments. Moreover, the effective area of contact improved the packing of the composite and thereby enhances the charge injection at the interface causing current flow to increase.

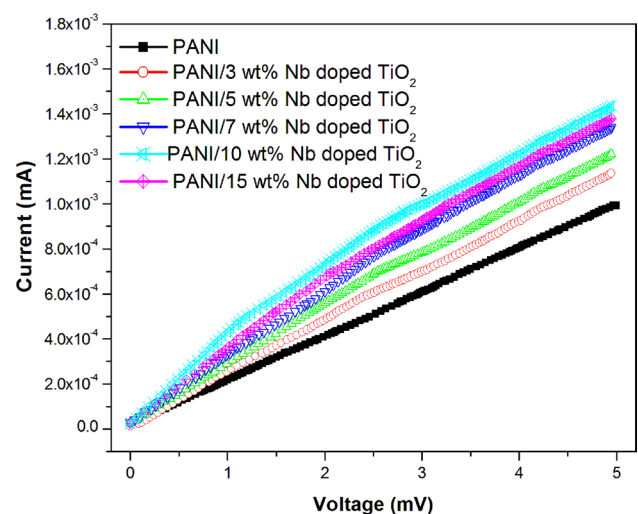


**Fig. 11** DC conductivity of PANI with different contents of Nb doped  $\text{TiO}_2$  nanoparticles at room temperature



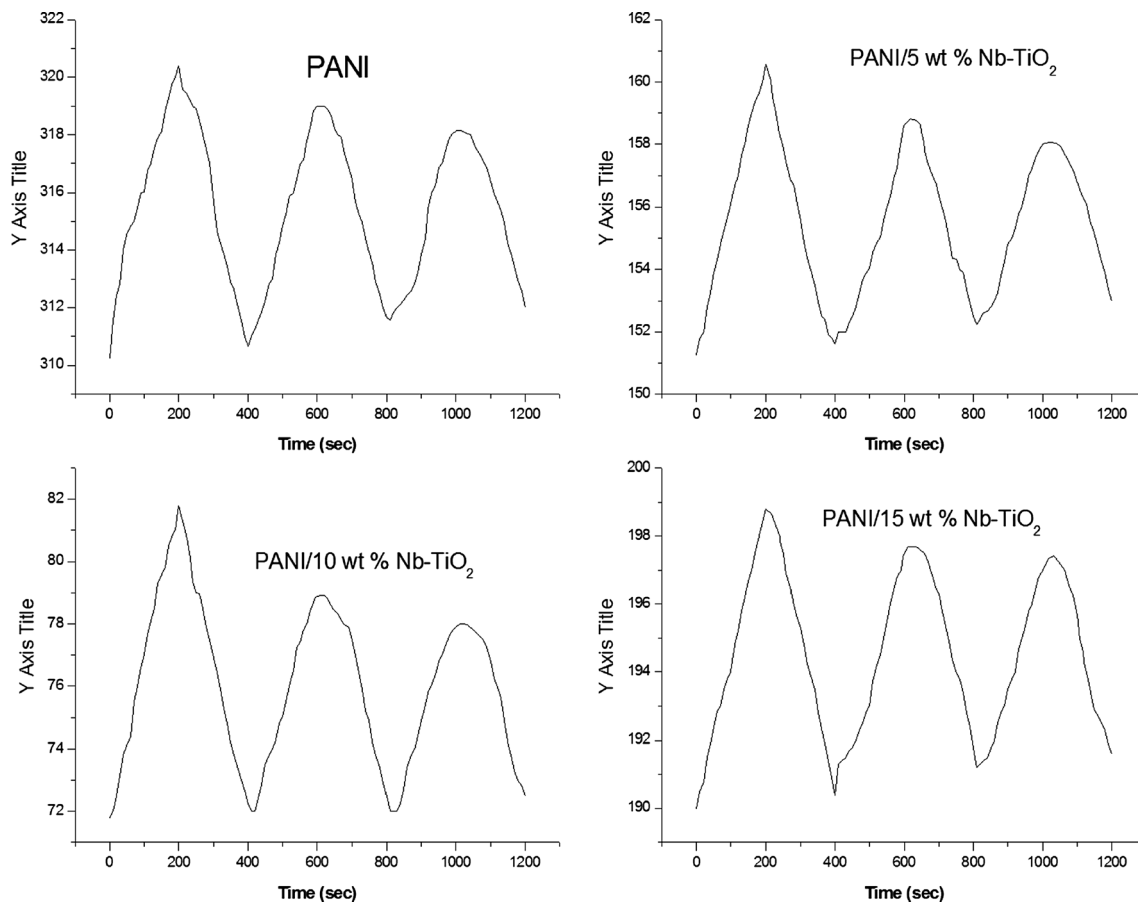
### 3.12 Gas sensing properties

Figure 12 shows the electrical resistance of PANI and PANI/Nb–TiO<sub>2</sub> nanocomposites as a function of exposing time of ammonia gas. The composite in the form of pellet is placed on silver plate inside the glass chamber and 100 ppm ammonia gas is passed into the chamber. The value of electrical resistance increases with the passage of ammonia gas with respect to time and the maximum resistance is observed for PANI. The higher resistance value of PANI can be attributed to the amorphous nature of polymer with the interaction of ammonia gas as compared to nanocomposites. The sensing mechanism can be explained by the protonation/deprotonation phenomena [36]. On repeating sensing cycles with constant ammonia concentration, it can be seen that the initial resistance starts on increasing and response resistance is found to be decreases. The initial resistance could not come back to original value. This could be due to the trapping of ammonia molecules on surface of composite. The graph showed that the resistance of the samples decreases with the addition of nanoparticles at a particular concentration (10 wt% Nb–TiO<sub>2</sub>). The lower

resistance value of 10 wt% sample is attributed to the less available interaction sites for ammonia gas or more specifically the interfacial interaction between polymer and filler particle is highest at this loading, which is already confirmed from the XRD, SEM and conductivity studies. The change in the sensor response of PANI and PANI/Nb–TiO<sub>2</sub> composites at room temperature with ammonia is shown in Fig. 13. The sensitivity of the nanocomposite increases linearly with the exposure of ammonia gas and the sensitivity of composite is higher than that of pure PANI. It is also clear from the figure that the sensing ability of the composite decreases at higher loading of nanoparticles (15 wt%) and this is either through the agglomeration of nanoparticles or by charge neutralization by the nanocomposite.

### 4 Conclusions

PANI/Nb–TiO<sub>2</sub> nanocomposites were successfully synthesized by incorporating Nb–TiO<sub>2</sub> nanoparticles into the PANI matrix by a simple in situ polymerization technique. The FT-IR and UV spectra confirmed the



**Fig. 12** Gas sensing response for ammonia gas of PANI and PANI with various contents of Nb doped TiO<sub>2</sub> nanoparticles

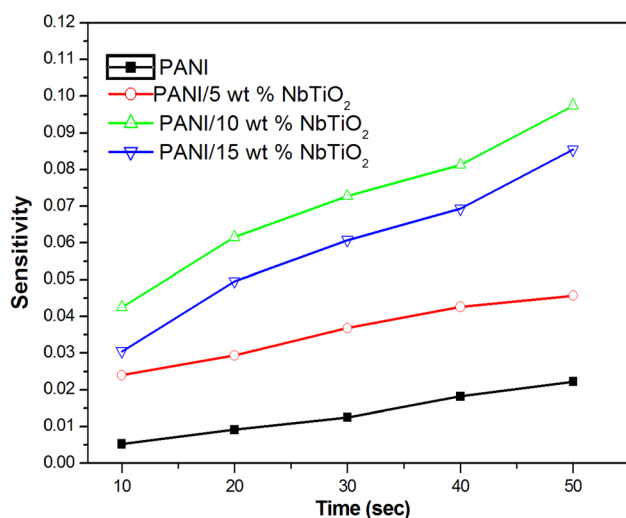


**Fig. 13** Change in gas sensitivity of PANI and PANI with different contents of Nb–TiO<sub>2</sub> nanoparticles at room temperature

interaction of nanoparticles with PANI through the shift and change in intensity or broadness of the spectrum. The addition of nanoparticles to PANI increases the systematic arrangement of polymeric structure and the ordered arrangement of chain increases with increase in concentration of nanoparticles. The morphological studies obtained from HRTEM and SEM (7 wt% composite) revealed that the nanoparticles were uniformly dispersed in the PANI with spherical shaped particles. However at higher content of nanoparticles (15 wt%) the uniform morphology is slightly changed into a tunnel spherical or enlarged molecules, indicated the formation of cluster within the PANI matrix. The increased glass transition temperature of composite with increase in concentration of nanoparticles results from the enhanced interaction between nanoparticles and the polymer chain. The rate of thermal decomposition of nanocomposite was poor as compared to PANI and the thermal stability increases with increase in loading of nanoparticles. The electrical properties such as AC conductivity, DC conductivity, dielectric constant and dielectric loss of nanocomposites were increased with the content of nanoparticles up to 10 wt% and thereafter the electrical properties decreased with further addition of fillers. The response of PANI/Nb–TiO<sub>2</sub> nanocomposite towards ammonia gas was found to be different with the loading of nanoparticles and the maximum sensing ability was observed for 10 wt% of composite. The prepared nanocomposites showed sensing ability to ammonia and good electrical properties and therefore this composite is a promising material for sensor, nanoelectronic devices and various electromagnetic shielding.

**Acknowledgements** The authors wish to thank Prof. P. P. Pradyumn, Department of Physics, University of Calicut, and Prof. P. Pradeep, Department of Physics, NIT Calicut, for providing necessary facilities in the department.

## References

1. Y. Yang, L. Zhang, S. Li, W. Yang, J. Xu, Y. Jiang, J. Wen, Electrochemical performance of conducting polymer and its nanocomposites prepared by chemical vapor phase polymerization method. *J. Mater. Sci.* **24**, 2245–2253 (2013)
2. M.T. Ramesan, V. Nidhisha, P. Jayakrishnan, Facile synthesis, characterization and material properties of novel poly (vinyl cinnamate)/nickel oxide nanocomposites. *Polym. Int.* **66**, 548–556 (2017)
3. M.T. Ramesan, V. Nidhisha, P. Jayakrishnan, Synthesis, characterization and conducting properties of novel poly (vinyl cinnamate)/zinc oxide nanocomposites via in situ polymerization. *Mater. Sci. Semicond. Process.* **63**, 253–260 (2017)
4. S.E. Gamal, A.M. Ismail, R.E. Mallowany, Dielectric and nanoscale free volume properties of polyaniline/polyvinyl alcohol nanocomposites. *J. Mater. Sci.* **26**, 7544–7553 (2015)
5. N. Pud, A. Ogurtsov, G. Korzhenko, Shapoval, Some aspects of preparation methods and properties of polyaniline blends and composites with organic polymers. *Prog. Polym. Sci.* **28**, 1701–1753 (2003)
6. M.O. Ansari, F. Mohammad, Thermal stability of HCl-doped polyaniline and TiO<sub>2</sub> nanoparticles-based nanocomposites. *J. Appl. Polym. Sci.* **124**, 4433–4442 (2012)
7. R. Sainz, A.M. Benito, M.T. Martínez, J.F. Galindo, J. Sotres, A.M. Baró, B. Corraze, O. Chauvet, A.B. Dalton, R.H. Baughman, A soluble and highly functional polyaniline-carbon nanotube composite. *Nanotechnology* **16**, 150–154 (2005)
8. J. Jang, J. Bae, M. Choi, S.H. Yoon, Fabrication and characterization of polyaniline coated carbon nanofiber for supercapacitor. *Carbon* **43**, 2730–2736 (2005)
9. W. Wang, A. H. Jayatissa, Comparison study of graphene based conductive nanocomposites using poly (methyl methacrylate) and polypyrrole as matrix materials. *J. Mater. Sci.* **26**, 7780–7783 (2015)
10. H. He, J. Zhu, N.J. Tao, L.A. Nagahara, I. Amlani, R. Tsui, A conducting polymer nanojunction switch. *J. Am. Chem. Soc.* **123**, 7730–7731 (2001)
11. N. Tessler, V. Medvedev, M. Kazes, S.H. Kan, U. Banin, Efficient near-infrared polymer nanocrystal light-emitting diodes. *Science* **295**, 1506–1508 (2002)
12. J.C. Chiang, A.G. MacDiarmid, Polyaniline: protonic acid doping of the emeraldine form to the metallic regime. *Synth. Met.* **13**, 193–205 (1986)
13. M.T. Ramesan, Synthesis, characterization, and properties of new conducting polyaniline/copper sulfide nanocomposites. *Polym. Eng. Sci.* **54**, 438–445 (2014)
14. R. Gangopadhyay, A. De, Conducting polymer nanocomposites: a brief overview. *Chem. Mater.* **12**, 608–622 (2000)
15. M.T. Ramesan, P. Jayakrishnan, T. Sampreeth, P.P. Pradyumn, Temperature dependent AC electrical conductivity, thermal stability and different DC conductivity modelling of novel poly (vinyl cinnamate)/zinc oxide nanocomposites. *J. Therm. Anal. Calorim.* **129**, 135–145 (2017)
16. M.T. Ramesan, K. Surya, Synthesis, characterization and properties of cashew gum graft poly (acrylamide)/magnetite nanocomposites. *J. Appl. Polym. Sci.* **133**, 5431–5438 (2016)
17. D.M. Sarno, J.J. Martin, S.M. Hira, C.J. Timpson, J.P. Gaffney, W.E. Jones, Enhanced conductivity of thin film polyaniline by

- self-assembled transition metal complexes. *Langmuir* **23**, 879–884 (2007)
18. B. Chaoqing, Y. Yijun., G. Xue, Synthesis of conducting polyaniline/TiO<sub>2</sub> composite nanofibres by one-step in situ polymerization method. *J. Appl. Polym. Sci.* **104**, 21–26 (2007)
  19. D.C. Schnitzler, M.S. Meruvia, I.A. Hummelgen, A.J.G. Zarkin, Preparation and characterization of novel hybrid materials formed from (Ti, Sn)O<sub>2</sub> nanoparticles and polyaniline. *Chem. Mater.* **15**, 4658–4665 (2003)
  20. Y. Yu, B. Che, Z. Si, L. Li, W. Chen, G. Xue, Carbon nanotube/polyaniline core-shell nanowires prepared by in situ inverse microemulsion. *Synth. Met.* **150**, 271–277 (2005)
  21. S. Lee, J.H. Noh, H.S. Han, D.K. Yim, D.H. Kim, J.K. Lee, J.Y. Kim, H.S. Jung, K.S. Hong, Nb-doped TiO<sub>2</sub>: a new compact layer material for TiO<sub>2</sub> dye-sensitized solar cells. *J. Phys. Chem. C* **113**, 6878–6882 (2009)
  22. A.V. Manole, M. Dobromir, M. Girtan, G. Rusu, D. Luca, Preparation of Nb-doped TiO<sub>2</sub> films by the sol-gel method. *J. Mater. Sci. Lett.* **9**, 624–626 (1990)
  23. M.T. Ramesan, Synthesis, characterization, and conductivity studies of polypyrrole/copper sulfide nanocomposites. *J. Appl. Polym. Sci.* **128**, 1540–1546 (2013)
  24. E.T. Kang, K.G. Neoh, K.L. Tan, Polyaniline: a polymer with many interesting intrinsic redox states. *Prog. Polym. Sci.* **23**, 277–324 (1998)
  25. K. Suhailath, M.T. Ramesan, B. Naufal, P. Periyat, V.C. Jasna, P. Jayakrishnan, Synthesis, characterization, flame, thermal and electrical properties of poly (n-butyl methacrylate)/titanium dioxide nanocomposites. *Polym. Bull.* **74**, 671–688 (2017)
  26. L. Zhang, M. Wan, Polyaniline/TiO<sub>2</sub> composite nanotubes. *J. Phys. Chem. B* **107**, 6748–6753 (2003)
  27. H. Su, Y.T. Huang, Y.H. Chang, P. Zhai, N.Y. Hau, P.C.H. Cheung, W.T. Yeh, T.C. Wei, S.P. Feng, The synthesis of Nb-doped TiO<sub>2</sub> nanoparticles for improved-performance dye sensitized solar cells. *Electrochim. Acta* **182**, 230–237 (2015)
  28. M. Hasik, A. Drelinkiewicz, E. Wenda, C. Paluszkiwicz, S. Quillard, FTIR spectroscopic investigations of polyaniline derivatives–palladium systems. *J. Mol. Struct.* **596**, 89–99 (2001)
  29. M.T. Ramesan, Poly (ethylene-co-vinyl acetate)/magnetite nanocomposites: interaction of some liquid fuels, thermal and oil resistance studies. *Polym. Polym. Compos.* **23**, 85–92 (2015)
  30. P. Jayakrishnan, M.T. Ramesan, Studies on the effect of magnetite nanoparticles on magnetic, mechanical, thermal, temperature dependent electrical resistivity and DC conductivity modeling of poly (vinyl alcohol-co-acrylic acid)/Fe<sub>3</sub>O<sub>4</sub> nanocomposites. *Mater. Chem. Phys.* **186**, 513–522 (2017)
  31. M.T. Ramesan, V.K. Athira, P. Jayakrishnan, C. Gopinathan, Preparation, characterization, antibacterial and electrical properties of sericin/poly (vinyl alcohol)/poly (vinyl pyrrolidone) composites. *J. Appl. Polym. Sci.* **133**, 5827–5836 (2016)
  32. P. Jayakrishnan, M.T. Ramesan, Synthesis, structural, magneto-electric and thermal properties of poly (anthranilic acid)/magnetite nanocomposites. *Polym. Bull.* **74**, 3179–3198 (2017)
  33. M.T. Ramesan, A. George, P. Jayakrishnan, G.K. Prasad, Role of pumice particles in the thermal, electrical and mechanical properties of poly (vinyl alcohol)/poly (vinyl pyrrolidone) composites. *J. Therm. Anal. Calorim.* **126**, 511–519 (2016)
  34. M.T. Ramesan, Raheem V.P.A., P. Jayakrishnan, P. P. Pradyumn, Acrylonitrile butadiene rubber (NBR)/manganous tungstate (MnWO<sub>4</sub>) nanocomposites: characterization, mechanical and electrical properties. *AIP Conf. Proc.* **1620**, 3–9 (2014)
  35. M.T. Ramesan, P. Jayakrishnan, Role of nickel oxide nanoparticles on magnetic, thermal and temperature dependent electrical conductivity of novel poly (vinyl cinnamate) based nanocomposites: applicability of different conductivity models. *J. Inorg. Organomet. Polym.* **27**, 143–153 (2017)
  36. M.C. Santos, A.G.C. Bianchi, D.M. Ushizima, F.J. Pavinatto, R.F. Bianchi, Ammonia gas sensor based on the frequency-dependent impedance characteristics of ultrathin polyaniline films. *Sens. Actuators A* **253**, 156–164 (2017)